Journal of Alloys and Compounds 509S (2011) S698–S704

Contents lists available at ScienceDirect

Journal of Alloys and Compounds

journal homepage: www.elsevier.com/locate/jallcom

Structural studies of lithium zinc borohydride by neutron powder diffraction, Raman and NMR spectroscopy

D.B. Ravnsbæk[a], C. Frommen[b], D. Reed[c], Y. Filinchuk[a,d,e], M. Sørby[b], B.C. Hauback[b], H.J. Jakobsen[f], D. Book[c], F. Besenbacher[g], J. Skibsted[f], T.R. Jensen[a,*]

[a] Center for Materials Crystallography (CMC), Interdisciplinary Nanoscience Center (iNANO), Department of Chemistry, Aarhus University, Langelandsgade 140, DK-8000 Aarhus C, Denmark
[b] Institute for Energy Technology, P.O. Box 40, N-2027 Kjeller, Norway
[c] School of Metallurgy and Materials, University of Birmingham, Edgbaston, Birmingham, B15 2TT, United Kingdom
[d] Swiss-Norwegian Beam Lines at ESRF, BP-220, 38043 Grenoble, France
[e] Institute of Condensed Matter and Nanosciences, Université Catholique de Louvain, 1 Place L. Pasteur, B-1348, Louvain-la-Neuve, Belgium
[f] Instrument Centre for Solid-State NMR Spectroscopy and Interdisciplinary Nanoscience Center (iNANO), Department of Chemistry, Aarhus University, Langelandsgade 140, DK-8000 Aarhus C, Denmark
[g] Interdisciplinary Nanoscience Center (iNANO) and Department of Physics and Astronomy, Aarhus University, Ny Munkegade 120, DK-8000 Aarhus C, Denmark

ARTICLE INFO

Article history:
Received 23 September 2010
Received in revised form 24 October 2010
Accepted 1 November 2010
Available online 11 November 2010

Keywords:
Metal borohydrides
Crystal structure
Neutron diffraction
Raman Spectroscopy
NMR spectroscopy

ABSTRACT

The crystal structure of $LiZn_2(BH_4)_5$ is studied in detail using a combination of powder neutron diffraction (PND), Raman spectroscopy, and ^{11}B MAS NMR spectroscopy on $LiZn_2(BH_4)_5$ and $LiZn_2(^{11}BD_4)_5$. The aim is to obtain detailed structural knowledge of the first interpenetrated framework hydride compound, $LiZn_2(BD_4)_5$ which consists of doubly interpenetrated 3D frameworks built from dinuclear complex ions $[Zn_2(BD_4)_5]^-$ and lithium ions. The positions of the deuterium atoms are determined using Rietveld refinement of the PND data and the orientation of one of the four independent BD_4^- groups is revised. The current data reveal that the structure of $[Zn_2(BD_4)_5]^-$ is more regular than previously reported, as are also the coordinations around the Zn and Li atoms. Both Zn and Li atoms are found to coordinate to the BD_4^- units via the tetrahedral edges. Some distortion of the angles within the BD_4 units is observed, relative to the expected angles of 109.4 for the ideal tetrahedral coordination. Raman spectroscopy confirms bending and stretching modes from the expected terminal and bridging bidentate BH_4^- and BD_4^- units. The ^{11}B MAS NMR spectrum of the satellite transitions resolves two distinct manifolds of spinning sidebands, which allows estimation of the ^{11}B quadrupole coupling parameters and isotropic chemical shifts for the four distinct ^{11}B sites of $[Zn_2(BD_4)_5]^-$. These parameters agree favorably well with the isotropic triple-quantum shifts, observed in an ^{11}B MQMAS NMR experiment. The present results may aid in the development and understanding of new borohydride materials for applications as fast ion conductors or as materials for hydrogen storage.

1. Introduction

Borohydride materials have received much attention recently due to their possible applications as fast ion conductors or as materials for hydrogen storage owing to their high gravimetric hydrogen densities [1–3]. Recently, lithium zinc borohydride has been utilized as a safe store of the poisonous gas diborane [4]. The borohydride chemistry is rich both regarding the reactivity and regarding the chemical bonding, which is mostly ionic for alkali metal borohydrides but more covalent for compounds based on *d*-block metals. However, the thermodynamic and kinetic properties of the metal borohydrides for hydrogen release and uptake are typically less attractive.

Recently, a wide range of novel metal borohydrides have been characterized structurally, physically and chemically and an empirical correlation between the decomposition temperature or the enthalpy of formation and the Pauling electronegativity of the cation was revealed [5]. These studies suggest that the introduction of more covalent bonding in borohydrides facilitates release of hydrogen at lower temperatures and also the formation of more open structures, e.g. $Mg(BH_4)_2$ [6], $Mn(BH_4)_2$ [7] and $Y(BH_4)_3$ [8–10] This relation also holds for a range of new bimetal borohydride, e.g. $LiK(BH_4)_2$ [11], $MSc(BH_4)_4$ (M = Li, Na and K) [12–14], $NaZn(BH_4)_3$, $MZn_2(BH_4)_5$ (M = Li or Na) [15] as well as the

* Corresponding author. Tel.: +45 89423894; fax: +45 86196199.
E-mail address: trj@chem.au.dk (T.R. Jensen).

0925-8388/$ – see front matter © 2010 Elsevier B.V. All rights reserved.
doi:10.1016/j.jallcom.2010.11.008

first structurally ordered heteroleptic borohydride, $KZn(BH_4)Cl_2$ [16].

These novel borohydrides exhibit a variety of different types of structures typically forming three dimensional frameworks, but large composite anions are also observed, e.g. $[Sc(BH_4)_4]^-$ and $[Zn(BH_4)Cl_2]^-$ [12–14,16] Moreover, the novel zinc-based borohydrides $MZn_2(BH_4)_5$ (M = Li or Na) exhibit fascinating novel structural motifs build of doubly interpenetrated 3D frameworks consisting of dinuclear complex anions $[Zn_2(BH_4)_5]^-$ and Li^+ or Na^+, acting as counter ions. This structural architecture has previously only been observed for coordination polymers involving organic ligands, also known as metal organic frameworks (MOFs) [17].

In this study, we focus on the detailed structure of the dinuclear complex ion $[Zn_2(BH_4)_5]^-$ in $LiZn_2(BH_4)_5$ combining information from three complementary techniques: powder neutron *diffraction* and Raman and NMR *spectroscopy*. The goal of the present study is to gain insight into the coordination of hydrogen atoms in the structure of the $LiZn_2(BH_4)_5$ and to obtain a more complete description of the metal-hydrogen bonds present in this material. This information may hold the key to obtain a more detailed understanding of the first example of a hydride interpenetrated framework.

2. Experimental

2.1. Sample preparation

All sample handling and preparations were performed under inert argon atmosphere in a MBraun Unilab glove box fitted with a recirculation gas purification system and gas/humidity sensors. Oxygen and water levels were kept well below 1 ppm during all operations.

Sample A (prepared at IFE): $LiZn_2(^{11}BD_4)_5$ was prepared from a mixture of double isotopically substituted $Li^{11}BD_4$ (>98%, Katchem) and $ZnCl_2$ (99.9% Aldrich) in a ratio of 2.5:1 milled in a Spex 6750 freezer-mill at liquid nitrogen temperature for 5 h. The mill was equipped with a stainless steel vial and impactor, and milling was performed with an agitation frequency of about 30 Hz for periods of 15 min each, followed by a 3 min cool-down time.

Samples B: $LiZn_2(BH_4)_5$ and C: double isotopically substituted $LiZn_2(^{11}BD_4)_5$ (prepared at Aarhus University) were prepared from mixtures of $LiBH_4$ (≥90%, Aldrich) or $Li^{11}BD_4$ (>98%, Katchem), respectively and $ZnCl_2$ (≥98%, Aldrich) in molar ratio 2:1. Both samples were ball milled in a Fritch Pulverisette No. 4 using the same procedure, i.e. high energy ball milling under inert conditions (argon atmosphere) comprised of 60 times 2 min of milling each intervened by 2 min breaks to avoid heating of the sample and a sample to ball ratio of approximately 1:35. All samples contained $LiZn_2(BH_4)_5$ or $LiZn_2(BD_4)_5$, LiCl and small amounts of $ZnCl_2$ after ball milling.

2.2. Powder neutron diffraction (PND)

PND data were collected for sample **A** with the PUS instrument at the JEEP II reactor at Kjeller, Norway [18]. Neutrons with the wavelength λ = 1.5549 Å were obtained from a Ge(5 1 1) focusing monochromator. The detector unit consists of two banks of seven position-sensitive ^{3}He-detectors, each covering 20° in 2θ (binned in steps of 0.05°). Data were collected in the 2θ range 10–130° at T = 22 °C. The sample was placed in a rotating cylindrical vanadium sample holder (diameter 6 mm).

2.3. Structure refinement

Rietveld refinement was performed using the *GSAS* program [19]. Pseudo-Voigt functions were applied (constant wavelength profile function type 2), for which the Caglioti (U, V, W) terms, Scherer broadening as well as peak symmetry were refined. The background was modeled by fitting a 30 terms shifted Chebyschev polynomial to manually chosen points. Three different phases were refined for sample A: $LiZn_2(^{11}BD_4)_5$, LiCl (ICSD data file No. 26909) and $ZnCl_2$ (ICSD data file No. 26154). The latter two compounds showed no signs of significant differences from the structures reported in the ICSD files. The Rietveld refinement of the structure concluded that the sample contained about 43 wt% $LiZn_2(^{11}BD_4)_5$, 41 wt% LiCl, and 16 wt% $ZnCl_2$. The atomic positions for the heavier atoms: Li, B and Zn obtained from a previous SR-PXD experiment on $LiZn_2(BH_4)_5$ were taken as a starting point for the Rietveld refinement of the neutron diffraction data [15]. Soft constraints were used on the geometry of the BD_4-tetrahedra, with B–D distances initial set to 1.22 Å, and allowed to vary within 0.03 Å limits. The structure was allowed to relax within 0.2 σ around these starting values. Common isotropic displacement factors were refined for each sort of atoms.

The final refinement of the PND data (see supplementary Fig. S1) gave the following results for $LiZn_2(^{11}BD_4)_5$: space group *Cmca*; lattice parameters: $a = 8.6031(13)$, $b = 17.8876(4)$ and $c = 15.3598(3)$ Å. The agreement factors are $R_{wp} = 2.78\%$, $R_p = 2.22\%$, and $\chi^2 = 1.56$ (not corrected for background).

Table 1
Structural data for the orthorhombic mixed-metal borohydride $LiZn_2(^{11}BD_4)_5$ derived from PND data (this study) and for $LiZn_2(BH_4)_5$ from SR-PXD data.[24].

	From PND	From PXD
Compound	$LiZn_2(^{11}BD_4)_5$	$LiZn_2(BH_4)_5$
Space group	*Cmca*	*Cmca*
a (Å)	8.5936 (18)	8.6244 (3)
b (Å)	17.857 (6)	17.8970 (8)
c (Å)	15.346 (5)	15.4114 (8)
Z	8	8
V (Å^3)	2354.9 (11)	2378.76 (19)
M (g/mol)	233.00	211.93
T (K)	295	295

2.4. Raman spectroscopy

Raman spectroscopic measurements were performed on the samples B, $LiZn_2(BH_4)_5$ and C, $LiZn_2(BD_4)_5$ using a Renishaw InVia reflex spectrometer with a confocal microscope with a ×20 objective. The excitation laser had a power of ~2 mW and a wavelength of λ = 488 nm. An Instec HCS621 V cell was used for inert sample transfer and measurement in a flow of 100 mL/min argon at 1 bar.

2.5. Solid state MAS NMR spectroscopy

Solid-state ^{11}B MAS and MQMAS NMR spectra of $LiZn_2(BH_4)_5$ and $LiZn_2(BD_4)_5$ (samples B and C) were obtained on a Varian INOVA-300 (7.05 T) spectrometer using a home-built CP/MAS NMR probe for 5 mm o.d. rotors. The experiments used an ^{11}B rf field strength of $\gamma B_1/2\pi = 75$ kHz, a spinning speed of $\nu_R = 10.0$ kHz, and a 4-s relaxation delay. The MQMAS NMR spectrum was obtained with the three-pulse, z-filter sequence [20], employing $\gamma B_1/2\pi = 75$ kHz for the triple-quantum (3Q) excitation and conversion pulses and $\gamma B_1/2\pi = 25$ kHz for the soft z-pulse, 128 increments in the t_1 dimension, and a 72-step phase cycle. The NMR experiments were performed at ambient temperature using air-tight, end-capped zirconia rotors packed with the samples in a Ar-filled glovebox. The determination of the ^{11}B quadrupole coupling parameters was performed by least-squares fitting of simulated to experimental spinning sideband intensities using the STARS software package [21]. The ^{11}B isotropic chemical shifts are in ppm relative to neat $F_3B\,O(CH_2CH_3)_2$.

3. Results and discussion

3.1. Detailed crystal structure of $LiZn_2(^{11}BD_4)_5$

In the present study, PND data is utilized for a detailed structural investigation, which is somewhat complementary to the previous study using synchrotron radiation X-ray powder diffraction (SR-PXD) [15]. Hydrogen (H) is the weakest scatterer of X-rays of all elements, however, deuterium (D) is a strong scatterer of neutrons, i.e. thereby the exact structural positions of deuterium can be determined.

From the Rietveld refinement of the PND data for $LiZn_2(^{11}BD_4)_5$ (sample A) the atomic positions of the heavier Zn atom are found to be in full agreement with the structural information obtained from previous SR-PXD studies [15], in contrast to the positions of Li and B positions which slightly differ from the previous findings. Table 1 presents structural data for $LiZn_2(^{11}BD_4)_5$ compared to previous published SR-PXD results for $LiZn_2(BH_4)_5$ and the revised structure is shown in Fig. 1 (the atomic coordinates and displacement parameters are given in supplementary Table S1). The overall structural topology of $LiZn_2(BD_4)_5$ is preserved consisting of two interpenetrated 3D frameworks,. However a distortion of the previously proposed framework structure is observed from the refinement of the PND data.

The most significant difference between the structures obtained from PND and SR-PXD data, is that the orientation of the borohydride unit containing atom B2 has been revised. In the initial refinement of the published SR-PXD model [15] versus the PND data, very large positional discrepancies for the $B2D_4$ group were obtained. The refinement resulted in a large difference between the two Zn–D

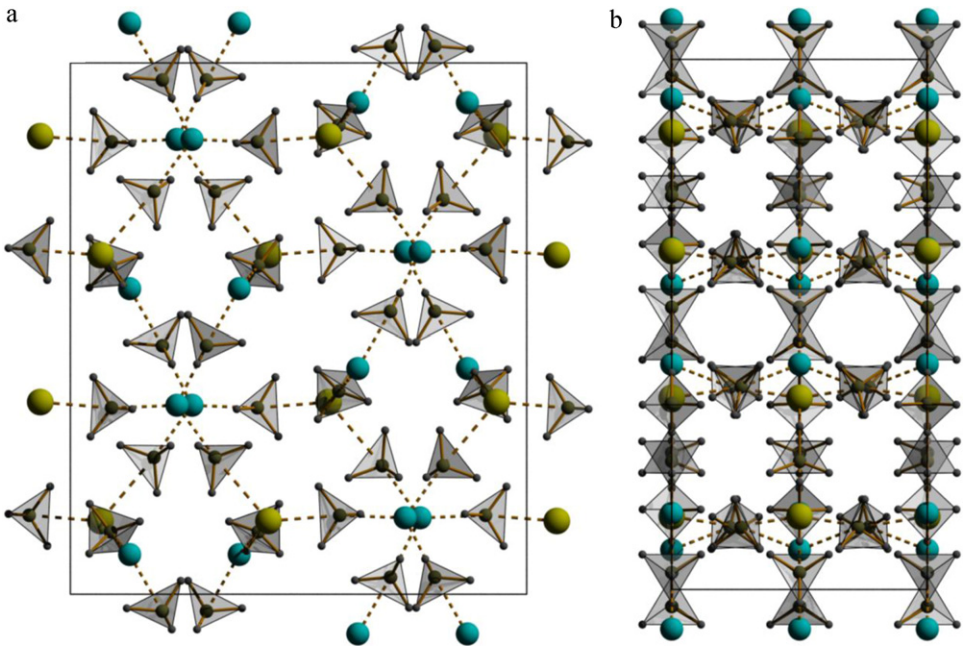

Fig. 1. The crystal structure of $LiZn_2(^{11}BD_4)_5$ viewed along (a) [1 0 0] and (b) [0 0 1] showing the three-dimensional framework. The B–D contacts are shown as solid bonds and BD_4-units are shown as transparent tetrahedra. Zn–B and Li–B contacts are shown as dashed lines. Metal-hydrogen bonds have been omitted for clarity (Zn blue, Li yellow, B brown and D gray).

distances. Furthermore, some of the Li–D distances involving the $B2D_4$ group were unrealistically short. Hence, the initial refinement suggested that the $B2D_4$ unit coordinates to Li via the tetrahedral face and to Zn via the tetrahedral vertex. Taking the coordination scheme of the other BD_4 units into account, this was found to be rather unlikely. Therefore, the $B2D_4$ unit was rotated by 90° around the *c*-axis connecting Zn and B atoms. This resulted in a better fit to the PND data decreasing the agreement from $R_{wp} = 3.59\%$, $R_p = 2.77\%$, and $\chi^2 = 2.07$ to $R_{wp} = 2.78\%$, $R_p = 2.22\%$, and $\chi^2 = 1.56$. Furthermore, this correction gave a much more regular coordination both around Li1 and Zn1. Also, the coordination environments for Zn1 and Zn2 atoms are identical in the revised structure.

Fig. 2 shows the local coordination of the two crystallographically independent Zn-atoms in $[Zn_2(BD_4)_5]^-$ with Zn–D contacts shown as bonds. Zn1 and Zn2 atoms have nearly planar trigonal environment considering the three Zn–B contacts. The plane of the Zn–B-triangle around Zn1 is orthogonal to the similar Zn–B triangle around Zn2.

The coordination mode for the BD_4 units to zinc in $[Zn_2(BD_4)_5]^-$ corresponds to the cation···D_2B coordination scheme, i.e. the BD_4 units share an edge with the zinc atoms. The observed coordination of the BH_4^- anion via the edge is typical for metal borohydrides [22]. It is interesting to note that the tentative hydrogen position found from PXD data for the anions $[Zn(BH_4)_3]_n^{n-}$ in $NaZn(BH_4)_3$ and $[Zn(BH_4)Cl_2]^-$ in $KZn(BH_4)Cl_2$ suggests that the coordination mode in these compounds also corresponds to the cation···H_2B scheme [15,16]. Thus, the preferred Zn–BH_4 coordination is likely to be edge sharing (η^2). On the other hand, for $[Sc(BH_4)_4]^-$ in $MSc(BH_4)_4$ M = Li, Na and K, the PXD data suggest that the coordination mode corresponds to the cation···H_3B scheme; that is, a BH_4^- unit has a face of three H atoms oriented towards the Sc (η^3) [12–14]. These results tend to indicate that it is the metal center and not the BH_4^- ligand that dictates the observed cation-BH_4 coordination. This suggests that the BH_4^- units act as a very flexible ligand, adapting to the coordination centre.

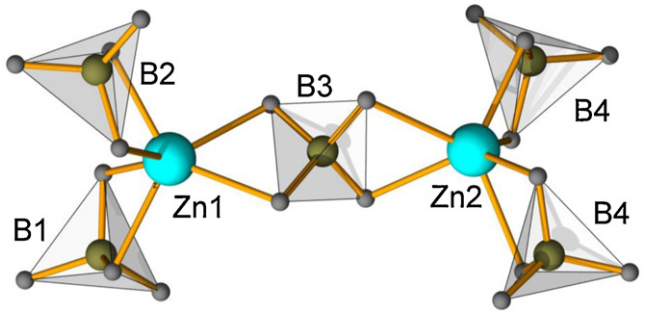

Fig. 2. Local coordination around the two different Zn-atoms in the $[Zn_2(BD_4)_5]^-$ anion. Zn–D and B–D contacts are represented as bonds.

The cation···D_2B coordination scheme in the $[Zn_2(BD_4)_5]^-$ anion results in a six-fold coordination of zinc to deuterium or, equivalently, three-fold coordination of Zn to η^2-BD_4^-. The coordination of zinc to deuterium forms trigonal prisms around Zn1 and Zn2 (see Fig. 3(a) and (b)). The BD_4 unit of B3 coordinates to both Zn1 and Zn2 via the two opposite tetrahedral edges. This type of nearly linear coordination of the BH_4 group via the opposite edges is typical for metal borohydrides, such as $Be(BH_4)_2$ [23], $Mg(BH_4)_2$ [6,24,25] and $Mn(BH_4)_2$ [7].

The interatomic distances and angles found in the final refinement (see supplementary Table S2) show a small spread, suggesting that the BD_4 tetrahedra are slightly distorted. Average values of bond lengths and angles are however, in accordance with previous studies of M-BH_4 compounds [22] and close to the expected value of 109.4 for the ideal tetrahedral coordination. While the deviations from the average B–D distance are statistically insignificant, the D–B–D angles in the Zn–D_2B and Li–D_2B fragments are slightly more open than for the non-coordinated D_2B edges. The average D–B–D angles are 112.4 and 115.9 respectively in the Zn–D_2B and Li–D_2B fragments, versus 107.3 for the D–B–D angles of the non-coordinating edges. Similar opening of the coordinated BH_2 edges was observed both experimentally by single crystal X-ray diffraction and by DFT calculations in α-$Mg(BH_4)_2$ ($P6_122$) and $Al(BH_4)_3$ [6,26–28]. While the experimental difference between the coordinated and non-coordinated H–B–H angles in $Mg(BH_4)_2$ is only 2.0°, the difference is 6.5° in $LiZn_2(BD_4)_5$. In fact, the D–B–D angles

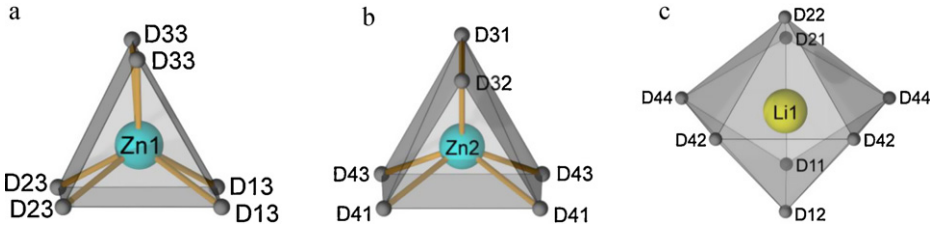

Fig. 3. (a) Trigonal prism showing the coordination of deuterium to Zn1 viewed along [1 0 0], (b) trigonal prism showing the coordination of deuterium to Zn2 viewed along [0 −1 −1] and (c) dodecahedron showing the coordination of deuterium to Li1 viewed along [0 1 0].

found for $LiZn_2(BD_4)_5$ by PND correspond very well to the 115(1)° and 107(1)° values obtained by DFT calculations for α-$Mg(BH_4)_2$ [29]. This reflects that the results obtained by PXD, are affected by the displacement of the electron cloud around the hydrogen atoms towards the metal, which results in observation of smaller opening angle. The positions of the nuclei are observed by PND, i.e. the actual opening angles are determined experimentally, and seem to confirm the results obtained by DFT calculations [29].

The Zn–D bonds from Zn1 are all similar, within the range from 1.799(16) to 1.835(18) Å. The Zn–D bonds involving Zn2 atom cover a wider range from 1.80(2) to 1.94(3) Å. The B-Zn–B angles are also similar, ranging from 116.5(9)° to 126.2(9)°, with the angles between the terminal BD_4^- units (B1, B2 and B4) larger than those between the terminal and bridging BD_4^- units. The bonding through Zn1–B3D_4–Zn2 define an almost linear coordination with an angle of 176.5(7).

The Li atom has a distorted saddle-like environment by four BD_4^- units, each from a different $[Zn_2(BD_4)_5]^-$ complex anion, hence Li connects the anionic fragments into a 3D framework. As for Zn, Li coordinates to the BD_4 tetrahedra in a bidentate fashion via the tetrahedral edges, i.e. the BD_4^- units act as η^2-ligands. Thus, Li coordinates to eight D-atoms forming distorted dodecahedra. This coordination is similar to that of Li in three of the four known $LiBH_4$ phases [30,31]. The Li–D bond lengths cover a very wide range from 1.88(7) to 2.639(11) Å.

As mentioned above, $LiZn_2(BD_4)_5$ consist of two interpenetrated 3D frameworks with no bonds between them. This is further underlined by looking separately at one of the two frameworks, containing 1D voids with coordinates *x*, 0.6014, 0.4090. The void radius, measured as the distance from the center to the nearest atom (deuterium), is 3.7 Å. It is similar in size to the empty voids found in α-$Mg(BH_4)_2$ [6] and the high-temperature phase of $Y(BH_4)_3$ [8,9]. In the structure of $LiZn_2(BD_4)_5$, these voids accommodate the second identical 3D framework.

3.2. Raman spectroscopy

Raman spectra of $LiZn_2(BH_4)_5$ (sample B) and $LiZn(BD_4)_5$ (sample C) are shown in Fig. 4. Table 2 lists the observed Raman shifts and the assignment for both $LiZn_2(BH_4)_5$ and $LiZn_2(BD_4)_5$. For $LiZn_2(BH_4)_5$ several bands are observed in the B–H stretching mode region from 2000 to 2600 cm^{-1}. Two maxima are observed at 2100 and 2458 cm^{-1}, corresponding respectively, to bidentate B–H stretching of the terminal B–H_2 and the B–H_2–Zn bridge in the terminal BH_4 units (B1, B2 and B4, Fig. 2) of $[Zn_2(BH_4)_5]^-$. Furthermore, additional weaker bands are observed between 2200 and 2400 cm^{-1}, which are assigned to bidentate B–H_2 stretching of the BH_4 unit bridging the two Zn atoms in the complex anion $[Zn_2(BH_4)_5]^-$. The observation of terminal B–H_2 stretching underlines that $[Zn_2(BH_4)_5]^-$ is an isolated anion, i.e. the coordination towards Li is much weaker. Between 990 and 1450 cm^{-1} three bands are observed most likely corresponding to B–H bending modes [32,33].

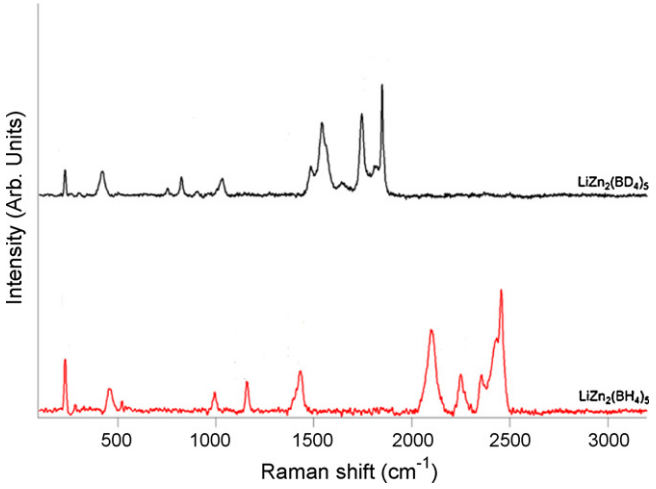

Fig. 4. Raman spectra of $LiZn_2(BH_4)_5$ (sample B) and $LiZn_2(^{11}BD_4)_5$ (sample C) measured at *RT* and with subtracted background.

The Raman spectrum of $LiZn_2(BD_4)_5$ (sample A) shows the same vibrations, though shifted to lower Raman frequencies due to the heavier deuterium atoms. Due to the *m*(H)/*m*(D) mass ratio of 1/2, the frequencies of the corresponding stretching in the tetrehedral

Table 2
Observed Raman shifts, shift ratios and assignments to specific bonds for $LiZn_2(BH_4)_5$ and $LiZn_2(BD_4)_5$.

Shift		Ratio	Assignment[a]
$LiZn_2(BH_4)_5$ (cm^{-1})	$LiZn_2(BD_4)_5$ (cm^{-1})	ω_D/ω_H	
2458	1848	0.752	Bidentate B–H_2 stretching, terminal BH_4 units (B1, B2, B4)
2356	1745	0.741	Bidentate B–H_2–Zn stretching, bridging BH_4 unit (B3)
2251	1569	0.697	Bidentate B–H_2–Zn stretching, bridging BH_4 unit (B3)
2100	1487	0.708	Bidentate B–H_2–Zn stretching, terminal BH_4 units (B1, B2, B4)
1431	1030	0.720	B–H bending
1159	825	0.712	B–H bending
995	740	0.743	B–H bending
470	430	–	Zn–B stretching
230	230	–	Zn–Cl vibrations in $ZnCl_2$

[a] B1, B2, B3 and B4 refer to the distinct BH_4 units shown in Fig. 2.

BD_4 is affected by the characteristic isotope shift factor of approximately 0.707 for an isotropic species [34]. These factors are found to range from 0.697 to 0.740 (see Table 2), indicating a small degree of anisotropy and that boron and possibly the surrounding Zn atoms take part in these internal vibrations as well.

Furthermore, bands are observed at 470 and 430 cm^{-1} for $LiZn(BH_4)_5$ and $LiZn_2(BD_4)_5$, respectively. These are assigned to Zn–B stretching, which corresponds well with the small observed isotope shift of this band, indicating that hydrogen and deuterium atoms take a small part in these vibrations. Similar Raman bands are observed for $MSc(BH_4)_4$ (M = Li, Na and K), which were assigned to Sc-B stretching modes [12–14]. Observation of such bands is indicative of isolated metal-borohydride complexes, since borohydrides containing no terminal BH_4 units e.g. $Mn(BH_4)_2$ and $Mg(BH_4)_2$ exhibit no Raman bands in this region [7,35]. The bands observed at 230 cm^{-1} for both samples are most likely related to Zn–Cl vibrations of the $Zn–Cl_4$ tetrahedra in $ZnCl_2$, which is present in small amounts in both samples.

3.3. Solid-state MAS NMR

The ^{11}B MAS NMR spectrum of the ^{11}B ($I = 3/2$) satellite transitions ($m = \pm 1/2 \leftrightarrow m = \pm 3/2$) for $LiZn_2(BD_4)_5$ (Fig. 5a) resolves two manifolds of spinning sidebands (ssbs), whereas three distinct peaks are observed in the isotropic dimension (F1) of the ^{11}B MQMAS NMR spectrum (Fig. 6). A ^{11}B MQMAS NMR spectrum of the non-deuterated sample ($LiZn_2(BH_4)_5$, sample B, not shown), obtained with ^1H decoupling in both the triple-quantum (3Q) evolution and single-quantum (1Q) detection periods, reveals the same resonances as observed in Fig. 6. However, the resolution is slightly better for the deuterated sample, which reflects that the strong ^{11}B–^1H dipolar couplings are not completely eliminated by MAS and ^1H decoupling under the present experimental conditions. Thus, the subsequent analysis focuses on the acquired spectra for $LiZn_2(BD_4)_5$. Examination of the ssb intensities in the MAS NMR spectrum clearly reveals that the manifold at lowest frequency exhibits the smallest quadrupole coupling and an overall intensity corresponding to roughly 20%. Furthermore, the line shapes of the ssbs in the manifold at high frequency include several shoulders and distinct peaks, indicating that this manifold is composed of resonances from two or more ^{11}B sites. Utilizing these distinct features in a least-squares fit of simulated to experimental ssb intensities for the satellite transitions, assuming that the high-frequency manifold contains resonances from three ^{11}B sites in a 1:1:2 ratio, results in the simulated MAS spectrum shown in Fig. 5b and the ^{11}B quadrupole coupling and isotropic chemical shift parameters listed in Table 3. Obviously, an unambiguous determination of these parameters is only achieved for the low-frequency site, as a result of the overlap of ssbs from the ^{11}B sites constituting the high-frequency ssb manifold. However, the ^{11}B parameters derived from the satellite transitions reproduce very well the isotropic triple-quantum chemical shifts (δ_{3Q}^{exp}) observed

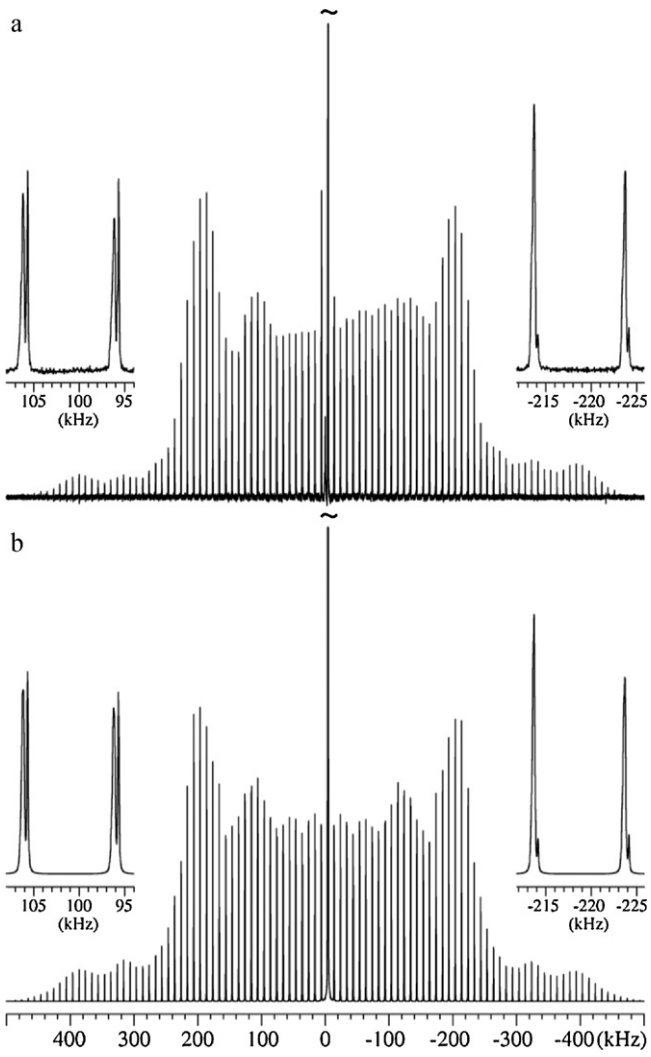

Fig. 5. (a) Experimental ^{11}B MAS NMR spectrum of $LiZn_2(BD_4)_5$, illustrating the manifold of ssbs from the satellite transitions, recorded at 7.05 T using a spinning speed of $\upsilon_R = 10.0$ kHz. (b) Optimized simulation of the ssb manifolds in (a), resulting in the ^{11}B quadrupole coupling parameters and isotropic chemical shifts listed in Table 3. The insets illustrate the splitting of the ssbs into two distinct manifolds.

in the ^{11}B MQMAS NMR spectrum (Fig. 6). These shifts can be calculated according to the relation [36]:

$$\delta_{3Q}^{calc} = \frac{17}{8}\delta_{iso} + \frac{1}{32}\frac{C_Q^2(1+\eta_Q^2/3)}{\nu_L^2} \times 10^6 \quad (1)$$

where υ_L is the ^{11}B Larmor frequency ($\upsilon_L = 96.24$ MHz at 7.05 T). The quadrupole coupling parameters are defined as $C_Q = (eQ/h)V_{zz}$ and $\eta_Q = (V_{yy} - V_{xx})/V_{zz}$, where Q is the nuclear quadrupole moment and V_{ii} the principal elements of the electric-field gradient ten-

Table 3
^{11}B Quadrupole coupling parameters (C_Q, η_Q), isotropic chemical shifts (δ_{iso}), and triple-quantum chemical shifts (δ_{3Q}) determined for $LiZn_2(BD_4)_5$[a].

δ_{iso} (ppm)	C_Q (kHz)	η_Q	Intensity	Assignment[b]	δ_{3Q}^{calc}[c] (ppm)	δ_{3Q}^{exp}[d] (ppm)
−42.3	945	0.09	1	B1	−87.0	−87.6
−43.1	748	0.32	1	B2	−89.7	−89.5
−43.3	879	0.06	2	B4	−89.4	−89.5
−46.0	553	0.19	1	B3	−96.7	−89.3

[a] The C_Q, η_Q, and δ_{iso} values are obtained from simulations of the ssb manifolds in Fig. 5a, assuming the presence of four ^{11}B sites with relative intensities of 1:1:1:2 (see text for further details).
[b] Assignment of the resonances to the four B sites in $LiZn_2(BD_4)_5$, reported from the PND data (Table S1).
[c] Isotropic triple-quantum chemical shifts, calculated from the C_Q, η_Q, and δ_{iso} values using Eq. (1).
[d] Isotropic triple-quantum chemical shifts, determined from the ^{11}B MQMAS spectrum in Fig. 6.

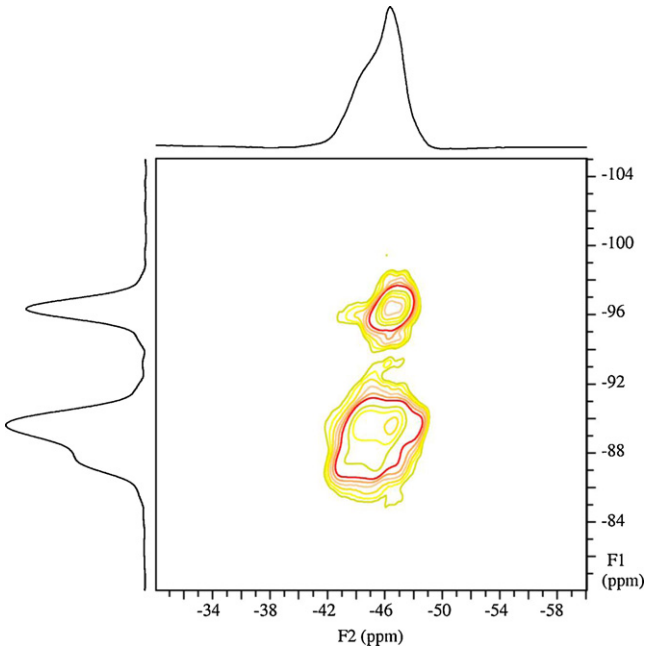

Fig. 6. ^{11}B MQMAS NMR spectrum (7.05 T, ν_R = 10.0 kHz) of $LiZn_2(BD_4)_5$, illustrating the resolution of three distinct ^{11}B sites in the isotropic dimension (F1). The vertical and horizontal spectra correspond to summations over the MQMAS spectrum in the isotropic (F1) and anisotropic (F2) dimensions, respectively. The isotropic 3Q shifts (δ_{3Q}^{exp}) determined from the vertical summation are listed in Table 3.

sor defined as $|V_{zz}| \geq |V_{xx}| \geq |V_{yy}|$. The experimental and simulated isotropic 3Q shifts are compared in Table 3, which reveal differences below 1 ppm for δ_{3Q}, which are below the error limit for this parameter, considering the uncertainty on the chemical shift reference and the resolution in the F1 dimension of the MQMAS experiment.

The present analysis shows that the ^{11}B MAS and MQMAS NMR spectra are in accord with the presence of four distinct sites in a 1:1:1:2 ratio for the $[Zn_2(BD_4)_5]^-$ anion. The coordination of the individual BD_4^- units in this anion, strongly suggests that the low-frequency resonance is assigned to the central BD_4^- unit (i.e., B3, Fig. 2), which has a unique coordination involving four B–D–Zn bonds. Furthermore, the relative intensities imply that the B4 site is associated with the δ_{iso} = −43.3 ppm resonance. The geometries of BD_4^- for the B1 and B2 sites (Table S2) indicate a higher degree of distortion for the BD_4^- tetrahedron of the B1 site, as evaluated by the average D–B–D bond-angle deviation from perfect tetrahedral symmetry. Thus, the B1 site is assigned to the δ_{iso} = −42.3 ppm resonance (Table 3) which exhibits the largest ^{11}B quadrupole coupling (tetrahedral distortion) of the two remaining resonances. An improved assignment and further insight into the relation between ^{11}B quadrupole coupling parameters and structural features of the BD_4^- units in the $[Zn_2(BD_4)_5]^-$ anion may potentially be achieved from density functional theory (DFT) calculations of the ^{11}B electric field gradients as demonstrated in a recent ^{11}B MAS NMR and DFT study of inorganic borates [37]. Finally, it is noted that the isotropic chemical shifts determined for $LiZn_2(BD_4)_5$ (Table 3) is very similar to the values reported for the zinc borhydrides $KZn(BH_4)Cl_2$ (δ_{iso} = −43.6 ppm) [16] and $NaZn(BH_4)_3$ (δ = −42.0 ppm and δ = −43.7 ppm in a 9.39 T) [15].

4. Conclusion

The detailed structure of $LiZn_2(BH_4)_5$ and $LiZn_2(BD_4)_5$ is investigated utilizing complementary techniques probing long range order, i.e. of powder neutron diffraction, and the first coordination spheres, i.e. Raman and MAS NMR spectroscopy. These studies show that the title compound contains a complex $[Zn_2(BH_4)_5]^-$ anion, where the BH_4 anion acts as a flexible but directional ligand. The complex anions and lithium cations are organized into a doubly interpenetrated framework. The refinement from PND diffraction data complements the results obtained by the previous SR-PXD studies, however, the coordination around both Li and Zn atoms is found to be more regular than previously depicted. The determination of the precise D-positions, results in revision of the orientation of one of the BD_4^- units and shows that the BD_4^- units act as η^2-ligands. Furthermore, it is revealed that the coordinated D_2B edges are slightly more open than the non-coordinated D_2B edges.

The Raman spectra support the PND data showing that there are BH_4 groups strongly coordinated by metal atoms in a bidentate η^2 mode. Furthermore, analysis of ^{11}B MAS and MQMAS NMR spectra of $LiZn_2(BD_4)_5$ is in accord with the presence of four different boron sites in the $[Zn_2(BD_4)_5]^-$ anion. The ^{11}B quadrupole coupling parameters and isotropic chemical shifts, reported for the four boron sites, are tentatively assigned to the different BD_4^- units reported from the PND data.

The thorough structural analysis of mixed metal borohydrides reveals the fascinating and complex structural chemistry of these compounds that can be described in terms of coordination chemistry. It gives new ideas for design and synthesis of other novel borohydride materials for applications as fast ion conductors or as materials for hydrogen storage.

Acknowledgments

We gratefully acknowledge the Danish Council for Independent Research|Natural Sciences (Danscatt), the Danish National Research Foundation (Centre for Materials Crystallography), the Danish Strategic Research Council (Centre for Energy Materials) and the Carlsberg Foundation for funding. The NANOMAT program of the Research Council of Norway is gratefully acknowledged for financial support. The use of the facilities at the Instrument Centre for Solid-State NMR Spectroscopy, Aarhus University, sponsored by the Danish Council for Independent Research|Natural Sciences, the Danish Technical Science Research Council, Teknologistyrelsen, The Carlsberg Foundation and Director Ib Henriksens Foundation, is acknowledged.

Appendix A. Supplementary data

Supplementary data associated with this article can be found, in the online version, at doi:10.1016/j.jallcom.2010.11.008.

References

[1] S.-I. Orimo, Y. Nakamori, J.R. Eliseo, A. Züttel, C.M. Jensen, Chem. Rev. 107 (2007) 4111–4132.
[2] W. Grochala, P.P. Edwards, Chem. Rev. 104 (2004) 1283–1315.
[3] H. Maekawa, M. Matsuo, H. Takamura, M. Ando, Y. Noda, T. Karahashi, S.-I. Orimo, J. Am. Chem. Soc. 131 (2009) 894–895.
[4] O. Friedrichs, A. Borgschulte, S. Kato, F. Buchter, R. Gremaud, A. Remhof, A. Züttel, Chem. Eur. J. 15 (2009) 5531–5534.
[5] Y. Nakamori, K. Miwa, A. Ninomiya, H.-W. Li, N. Ohba, S. Towata, A. Züttel, S.-I. Orimo, Phys. Rev. B 74 (2006) 045126.
[6] Y. Filinchuk, R. Černý, H. Hagemann, Chem. Mater. 21 (2009) 925–933.
[7] R. Černý, N. Penin, H. Hagemann, Y. Filinchuk, J. Phys. Chem. C 113 (2009) 9003–9007.
[8] D.B. Ravnsbæk, Y. Filinchuk, R. Černý, M.B. Ley, D. Haase, H.J. Jakobsen, J. Skibsted, T.R. Jensen, Inorg. Chem. 49 (2010) 3801–3809.
[9] C. Frommen, N. Aliouane, S. Deledda, J.E. Fonneløp, H. Grove, K. Lieutenant, I. Llamas-Jansa, S. Sartori, M.H. Sørby, B.C. Hauback, J. Alloys Compd. 496 (2010) 710–716.
[10] T. Jaron, W. Grochala, Dalton Trans. 39 (2010) 160–166.
[11] E.A. Nickels, M.O. Jones, W.I.F. David, S.R. Johnson, R.L. Lowton, M. Sommariva, P.P. Edwards, Angew. Chem. Int. Ed. 47 (2008) 2817–2819.

[12] H. Hagemann, M. Longhini, J.W. Kaminski, T.A. Wesolowski, R. Černý, N. Penin, M.H. Sørby, B.C. Hauback, G. Severa, C.M. Jensen, J. Phys. Chem. A 112 (2008) 7551–7555.
[13] R. Černý, G. Severa, D.B. Ravnsbæk, Y. Filinchuk, V. d'Anna, H. Hagemann, D. Haase, C.M. Jensen, T.R. Jensen, J. Phys. Chem. C 114 (2010) 1357–1364.
[14] R. Černý, D.B. Ravnsbæk, G. Severa, Y. Filinchuk, V. d'Anna, H. Hagemann, D. Haase, J. Skibsted, C.M. Jensen, T.R. Jensen, J. Phys. Chem. C 114 (2010) 19540–19549.
[15] D. Ravnsbæk, Y. Filinchuk, Y. Cerenius, H.J. Jakobsen, F. Besenbacher, J. Skibsted, T.R. Jensen, Angew. Chem. Int. Ed. 48 (2009) 6659–6663.
[16] D.B. Ravnsbæk, L.H. Sørensen, Y. Filinchuk, D. Reed, D. Book, H.J. Jakobsen, F. Besenbacher, J. Skibsted, T.R. Jensen, J. Eur. Inorg. Chem. (2010) 1608–1612.
[17] T.K. Maji, R. Matsuda, S.A. Kitagawa, Nat. Mater. 6 (2007) 142–148.
[18] B.C. Hauback, H. Fjellvåg, O. Steinsvoll, K. Johansson, O.T. Buset, J. Jørgensen, J. Neutron Res. 8 (2000) 215–232.
[19] A.C. Larson, R.B. Von Dreele, General Structure Analysis System (GSAS), Los Alamos National Laboratory Report LAUR (2004) 86–748.
[20] J.-P. Amoureux, C. Fernandez, S. Steuernagel, S. J. Magn. Reson. Ser. A 123 (1996) 116–118.
[21] J. Skibsted, N.C. Nielsen, H. Bildsøe, H.J. Jakobsen, J. Magn. Reson. 95 (1991) 88–117.
[22] Y. Filinchuk, D. Chernyshov, V. Dmitriev, Z. Kristallogr. 223 (2008) 649–659.
[23] D.S. Marynick, W.N. Lipscomb, Inorg. Chem. 11 (1972) 820–823.
[24] R. Černý, Y. Filinchuk, H. Hagemann, K. Yvon, Angew. Chem. Int. Ed. 46 (2007) 5765–5767.
[25] J.H. Her, P.W. Stephens, Y. Gao, G.L. Soloveichik, J. Riissenbeek, M. Andrus, J.C. Zhao, Acta Cryst. B 63 (2007) 561–568.
[26] B. Dai, D.S. Sholl, J.K. Johnson, J. Phys. Chem. C 112 (2008) 4391–4395.
[27] S. Aldridge, A.J. Blake, A.J. Downs, R.O. Gould, S. Parsons, C.R. Pulham, J. Chem. Soc. Dalton Trans. (1997) 1007–1012.
[28] J.P. Soulié, G. Renaudin, R. Černý, K. Yvon, J. Alloys Compd. 346 (2002) 200–205.
[29] M.J. van Setten, G.A. de Wijs, M. Fichtner, G. Brocks, Chem. Mater. 20 (2008) 4952–4956.
[30] Y. Filinchuk, D. Chernyshov, R. Černý, J. Phys. Chem. C 112 (2008) 10579–10584.
[31] Y. Filinchuk, D. Chernyshov, A. Nevidomskyy, V. Dmitriev, Angew. Chem. Int. Ed. 47 (2008) 529–532.
[32] T.J. Marks, J.R. Kolb, Chem. Rev. 77 (1977) 263–293.
[33] R. Černý, K.C. Kim, N. Penin, V. D'Anna, H. Hagemann, D.S. Sholl, J. Phys. Chem. C 114 (2010) 19127–19133.
[34] G. Herzberg, Molecular Spectra and Molecular Structure, Infrared and Raman Spectra of Polyatomic Molecules, vol. 2, Krieger Publication Company, Malabar, FL, 1991.
[35] A. Giannasi, D. Colognesi, L. Ulivi, M. Zoppi, A.J. Ramirez-Cuesta, E.G. Bardají, E. Roehm, M.J. Fichtner, Phys. Chem. A 114 (2010) 2788–2793.
[36] D. Massiot, B. Touzo, D. Trumeau, J.P. Coutures, J. Virlet, P. Florian, P.J. Grandinetti, Solid State Nucl. Magn. Reson. 6 (1996) 73–83.
[37] M.R. Hansen, G.K.H. Madsen, H.J. Jakobsen, J. Skibsted, J. Phys. Chem. A 109 (2005) 1989–1997.